Theoretical study of trends in conductance for molecular junctions formed with armchair carbon nanotube electrodes

Yiing-Rei Chen*
Department of Chemistry, Columbia University, New York, New York 10027, USA
and Department of Physics, National Taiwan Normal University, Taipei 11677, Taiwan

Lei Zhang
Department of Chemistry, Columbia University, New York, New York 10027, USA
and Center for Electron Transport in Molecular Nanostructures, Columbia University, New York, New York 10027, USA

Mark S. Hybertsen†
Center for Functional Nanomaterials, Brookhaven National Laboratory, Upton, New York 11973, USA;
Department of Applied Physics and Applied Mathematics, Columbia University, New York, New York 10027, USA;
and Center for Electron Transport in Molecular Nanostructures, Columbia University, New York, New York 10027, USA
(Received 9 April 2007; published 10 September 2007)

The transmission through prototype aromatic molecule junctions formed between armchair (metallic) carbon nanotube electrodes is studied using a tight-binding model with a Green's function embedding approach. Analytical and numerical results for transmission near the Fermi energy are obtained for junctions of single molecules with a one-point contact to each electrode, pairs of such molecules in the junction, and double stranded molecules with a two-point contact to each electrode. While an ideal single stranded molecule (ideal polyene) with odd number of atoms gives unit transmission at the Fermi energy, two such strands in the junction demonstrate significant interference effects, with net transmission varying from near zero to near 2 depending on the specific contact sites at the electrodes. Ideal polyenes with even number of atoms give nonresonant single-molecule transmission at the Fermi energy and less pronounced interference effects from their double-molecule junctions. The bonded, two stranded junction (polyacene) also gives nonresonant transmission at the Fermi energy. Allowing for the more realistic bond alternation observed in aromatic molecules results in nonresonant transmission with exponential length dependence.

DOI: 10.1103/PhysRevB.76.115408 PACS number(s): 73.23.Ad, 73.63.Fg, 73.63.Rt

I. INTRODUCTION

Single-molecule junctions are generally formed in nanoscale gaps between conventional metal electrodes. The conductance is significantly affected by the connection between the molecule and the metal.[1] Most experiments are performed with gold electrodes, using a terminal thiol group to bond the molecule to the gold electrode surface.[2] This approach takes advantage of a broad base of experience in the formation of organic layers through the thiol-gold route to self-assembly.[3,4] Unfortunately, there is substantial variation in the measured conductance of molecular junctions formed with thiol links,[2] possibly due to changes in the local structure of the Au-S link in different junctions.[5] Some research has been directed to map out alternative electrode materials to support more selective link motifs, e.g., Ru or Mo carbene links.[6,7] Also, it has been recently demonstrated that amine linkages to gold electrodes form reliable junctions.[8–10] However, the reproducible formation of a well-defined electrode-molecule link remains a significant issue in the study of single-molecule junctions.

Single wall carbon nanotubes (CNTs) present an attractive alternative electrode for single-molecule junctions. Since their initial discovery,[11,12] these crystalline, quasi-one-dimensional materials have been widely studied. The structures are formed by rolling up a section of a single graphene sheet, a honeycomb network of sp^2 bonded carbon (C), to form a nanoscale tube. Depending on the orientation of the roll-up vector, either a metallic or a semiconducting band structure results.[13] The conducting properties of CNTs have been extensively studied and exploited to form novel electronic devices with a CNT acting as the conducting channel.[14,15] Recently, CNT electrodes have also been exploited to form the source and drain electrodes for transistor structures with nanoscale molecular assemblies forming the conducting channel.[16–18] However, the molecules in the channel of these structures are not directly bonded to the CNT electrodes.

In forming a single-molecule junction, the end of a CNT presents the possibility of a direct bond with a character very similar to the intramolecular bonding. This may lead to easier chemical control of the junction structure and a link with good continuity of electronic character between the electrode and the molecule in the junction. A specific procedure has now been demonstrated to fabricate a molecular scale gap in a CNT followed by insertion of selected molecules linked to the CNT via a dehydration reaction to form amide linkages.[19] Electrical characteristics of junctions formed by molecules bridging the CNT electrodes were measured and molecule specific conductance phenomena were observed.

A junction formed by a molecule covalently bonded to CNT electrodes presents two distinguishing features. First, in contrast to a conventional, bulk metal, the CNT electrode has

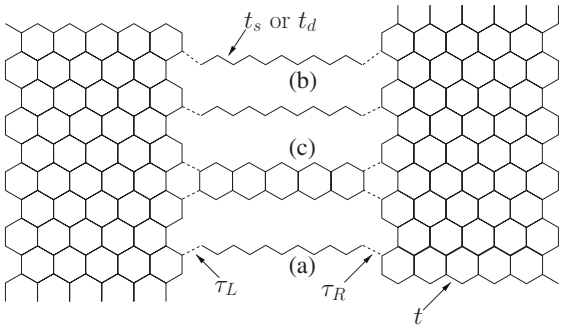

FIG. 1. Schematic two-dimensional illustration of the three classes of armchair CNT-molecule junction: (a) single polyene, (b) two parallel polyenes, and (c) polyacene with two points of attachment on each side. In a nearest neighbor TB model for the π electrons, the hopping energy is t within each CNT electrode, t_j within the molecule, and $\tau_{L,R}$ coupling the molecule to the electrodes.

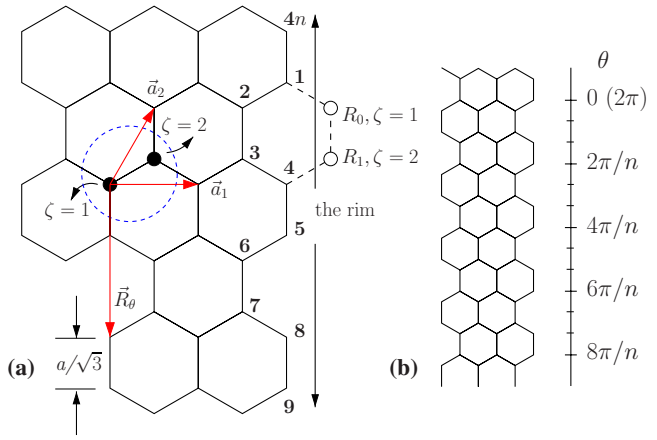

FIG. 2. (Color online) (a) Portion of an unwrapped (n,n) metallic CNT, back to the view of a graphene sheet, defining labels and notation used in the text. (b) Mapping the edge carbon atom sites to an angular measure θ around the circumference of the CNT end.

just two electronic channels (times two for spin) near the Fermi energy. Second, the character of the bonding in the electrode, in the molecule, and at the link can be very similar. In particular, the C π electron system in the electrodes that forms the states near the Fermi energy can directly couple to the π electron states in a molecule in the junction. One might then ask if the CNT-molecule junction is in some way more ideal. Under what circumstances does a bridging molecule attached to one C atom on each electrode restore a full conductance channel? If two identical molecules bridge the electrodes, under what conditions does the conductance double? If there are two points of attachment for a single molecule, are both channels of conductance restored? What is the influence of the CNT diameter?

We address aspects of these broad questions by examining model molecules bridging two armchair (metallic) CNTs in order to understand the basic trends in the low bias conductance of CNT-molecule junctions. We consider molecules that represent fragments of the sp^2 bonded C network of the CNT electrode. Specifically, different length polyenes (single strand) and polyacenes (double strands) are studied. We also consider two polyenes bridging the electrodes. These cases are illustrated in Fig. 1. We confine our attention to the π electron system treated within a nearest neighbor tight-binding model and simulate chemical differences at the link by a variable π electron coupling between the end of the CNT and the molecule. When the electronic coupling at the link and within the molecule region is identical to the electrode, one can think of the junction as being formed by selectively removing C atoms from an ideal CNT. By appropriate choice of the tight-binding parameters on the molecule, the more realistic situation of alternating double and single bond is simulated.

The conductance is evaluated using the Landauer approach with the transmission calculated using a Green's function embedding approach applied within the tight-binding (TB) model.[20] The TB model for the π electron system of the CNT electrodes captures the main features near the Fermi energy.[21] A similar approach has been applied to study transport through different structures composed of ribbons of graphene.[22–24] A scattering state approach, also based on a TB model, has been used to study transmission spectra for selected CNT-wire[25] and CNT-C_{60} (Ref. 26) junctions. A recent density functional theory (DFT) based study, including self-consistent potential effects, examined the I-V curve for a pseudopeptide bonded to semiconducting CNT electrodes, observing negative differential resistance.[27] In a related study, the impact of lattice fluctuations on ballistic transport through armchair CNT segments was small for energies near the Fermi energy, although more significant for higher energy channels.[28] In the present study, the high symmetry of the armchair CNT electrodes results in embedding self-energies with a compact form at energies near the Fermi energy. The relative simplicity of the TB model allows for analytical expressions describing the transmission at the Fermi energy for each of the cases illustrated in Fig. 1. Numerical calculations are used to present a picture of the self-energies and the transmission over a range of energies.

The rest of the paper is organized as follows. In Sec. II, the physical model and the theoretical methods are described, including the evaluation of the embedding self-energy that describes the coupling of the armchair CNT electrodes to the molecule. The transmission results for the different classes of bridging molecules are presented and discussed in Sec. III. Conclusions are presented in Sec. IV. Some background details for evaluating the CNT electrode Green's function appear in the Appendix.

II. MODEL AND THEORETICAL METHODS

A. Tight-binding model

In the experiments done to date,[19] the chirality and detailed geometry of the ends of the CNT electrodes are unknown. Here, the electrodes are assumed to be metallic armchair CNTs with ideal termination. These are conventionally labeled by the wrap-up indices (n,n). With reference to the edge illustrated in Fig. 2, there are n C-C pairs (e.g., 4 and 5) at the end of the (n,n) CNT. In the schematic picture of the model junctions (Fig. 1), we assume that all the dangling σ

bonds implicit in the C sites that are twofold coordinated have been saturated. Each C atom contributes one p orbital to the π system that is directly included in the TB model. We include only the nearest neighbor ($pp\pi$) hopping and assume a uniform hopping energy t throughout the CNT lead. A separate value τ couples the edge of the CNT electrodes to the central molecule. Finally, interior to the molecule, the values of the hopping energies are chosen to model different situations. For the ideal reconnection case, the values are uniform and equal to that in the CNT electrodes. To simulate the more realistic effect of bond alternation expected for finite chains, the values alternate as t_d, t_s. In general, a variation in the local potential would be expected in the region of the junction, depending in part on the details of the link bonding. Potential effects are not included. The on-site energy of each carbon atom in the CNT and the molecule is taken as a constant, equal to the CNT Fermi energy E_F, and $E_F \equiv 0$. While clearly an idealization, it simplifies the analysis of trends and enables some analytical results to be derived. In the matrix form, the Hamiltonian is indexed by the sites in the left CNT, the molecule, and the right CNT:

$$\mathcal{H}_{\text{total}} = \begin{pmatrix} \mathcal{H}_L & \tau_L^\dagger & 0 \\ \tau_L & \mathcal{H}_D & \tau_R \\ 0 & \tau_R^\dagger & \mathcal{H}_R \end{pmatrix}. \tag{1}$$

B. Green's function approach

In general, the Green's function embedding approach is useful in treating finite subsystems (e.g., the molecule here, $\mathcal{H}_D$) coupled to semi-infinite regions by a finite range interaction.[29] It also provides a straightforward connection to the conductance through the central region.[20] In the present case, the coupling matrices τ_L and τ_R have only a few nonzero elements. At the expense of also requiring part of the surface Green's function of the decoupled left and right electrodes,

$$g_{sL(R)}(E) = \lim_{\eta \to 0} [(E + i\eta)I - \mathcal{H}_{L(R)}]^{-1}, \tag{2}$$

the Green's function for the coupled system in the central molecule subspace can be derived:

$$G(E) = \lim_{\eta \to 0} [(E + i\eta)I - \mathcal{H}_D - \Sigma_L(E) - \Sigma_R(E)]^{-1}. \tag{3}$$

The influence of the coupling to the electrodes is captured through the self-energy functions which are calculated from the surface Green's functions of the CNT electrodes:

$$\Sigma_{L(R)}(E) = \tau_{L(R)} g_{sL(R)}(E) \tau_{L(R)}^\dagger. \tag{4}$$

The real parts of the self-energies shift molecular resonances, while the imaginary parts give the broadening due to the coupling to a continuum of states in the electrodes. Because of the finite range of the coupling matrices τ_L and τ_R, the self-energies are only nonzero over a finite range near the link to the electrodes. Similarly, only a finite range of the electrode surface Green's functions $g_{sL,R}$ are required. Further details are discussed in the next section.

Once the Green's function in the molecular region has been obtained, the imaginary part of the self-energy functions,

$$\Gamma_{L,R}(E) = i[\Sigma_{L,R}(E) - \Sigma_{L,R}^\dagger(E)], \tag{5}$$

gives the coupling that enters into the final formula for the current through the junction:[20]

$$I_L = \frac{1}{\hbar} \int \frac{dE}{2\pi} \text{Tr}(\Gamma_L G \Gamma_R G^\dagger)(f_L - f_R).$$

Here, the Fermi functions for the left and right electrode also enter, with the difference in the two chemical potentials corresponding to the applied bias. If we define the transmission $T \equiv \text{Tr}(\Gamma_L G \Gamma_R G^\dagger)$, then this is equivalent to the multichannel Landauer formula. In general, the applied bias must be included in the Hamiltonian as an appropriate potential distribution and the Green's function calculated for each bias level. Here, we focus on the low bias conductance (linear response regime):

$$\left. \frac{dI}{dV} \right|_{V=0} = \frac{2e^2}{h} T(0).$$

To compute the conductance for our model systems, within the TB model, we first require the surface Green's functions. These are discussed in the next section. With the restriction to nearest neighbor hopping, the nonzero elements of the self-energy span the number of attachment points. For the polyene case, it is a single function of energy for the left and for the right. For the polyacene, it is a 2×2 matrix for the left and for the right. For example, in the case of an M-atom polyene with equal bond lengths, the needed Green's function is the following M-dimensional matrix:

$$G(E) = \begin{pmatrix} E - \Sigma_L(E) & t & & & & & \\ t & E & t & & & & \\ & t & E & \ddots & & & \\ & & \ddots & \ddots & \ddots & & \\ & & & \ddots & E & t & \\ & & & & t & E - \Sigma_R(E) & \end{pmatrix}^{-1}. \tag{6}$$

The self-energies have an imaginary part, so unless specifically simulating a dephasing effect, we can safely set $\eta = 0$. The numerical results described in the next section are obtained by direct evaluation of $G(E)$.

In selected cases, a recursion technique can be applied to obtain analytical results due to the simple form of the Hamiltonian and the self-energies in the TB model. For example, for the M-atom polyene, the transmission depends only on one off-diagonal element of G:

$$T(E) = \Gamma_{L,11} G_{1M}(E) \Gamma_{R,MM} G_{1,M}(E)^*. \tag{7}$$

This off-diagonal element can be obtained by iteration of a block recursion scheme.[30] The Hamiltonian is divided into diagonal blocks and off-diagonal couplings between the blocks (e.g., the diagonal elements and the t's above). Recursion consists of sequentially adjoining blocks and updating

the needed diagonal $[G^{(j)}_{j,j}(E)]$ and off-diagonal $[G^{(j)}_{1,j}(E)]$ blocks of the Green's function for the intermediate system consisting of j blocks. For the uniform M-polyene illustrated above, the iterates in this scheme[30] are

$$G^{(j)}_{j,j}(E=0)=\begin{cases}\dfrac{-1}{\Sigma_L} & \text{if } j \text{ is odd}\\ \dfrac{\Sigma_L}{t^2} & \text{if } j \text{ is even,}\end{cases} \tag{8}$$

$$G^{(j)}_{1,j}(E=0)=\begin{cases}\dfrac{(-1)^{(j+1)/2}}{\Sigma_L} & \text{if } j \text{ is odd}\\ \dfrac{(-1)^{j/2}}{t} & \text{if } j \text{ is even.}\end{cases} \tag{9}$$

When assembled together, including the possibility that the self-energy on the right may be different, one obtains

$$T(E=0)=\frac{4\,\mathrm{Im}\,\Sigma_L\,\mathrm{Im}\,\Sigma_R}{|\Sigma_L+\Sigma_R|^2}, \quad M \text{ odd}, \tag{10}$$

$$T(E=0)=\frac{4\,\mathrm{Im}\,\Sigma_L\,\mathrm{Im}\,\Sigma_R t^2}{|\Sigma_L\Sigma_R-t^2|^2}, \quad M \text{ even}. \tag{11}$$

This approach has been used to supply the analytical results below.

C. Surface Green's function

In the present nearest neighbor TB model, we only require the surface Green's function in Eq. (2) evaluated at the atoms on the edge of the semi-infinite CNT end (e.g., atoms 1, 4, 5, etc., in Fig. 2). Furthermore, in this TB model with uniform hopping energies and on-site energies throughout the electrode, a recursive equation for the surface Green's function components can be set up and solved.[31] For the (n,n) armchair CNT, the recursion equations apply to the $4n\times 4n$ block spanning the atoms $1, 2, \ldots, 4n$ in Fig. 2. The recursion equations are solved numerically for each energy with care to choose a sufficiently small value of η (10^{-7}) and a strict criterion on the norm of the recursion error (10^{-12}) in the surface Green's function matrix.

Alternatively, the elements of the Green's function matrix in real space can be written in general in terms of the wave functions and eigenvalues for the semi-infinite CNT:

$$g_s(R,\zeta;R',\zeta';E)=\sum_{\mathbf{k}\lambda}\frac{\phi(\mathbf{k},\lambda;R,\zeta)\phi(\mathbf{k},\lambda;R',\zeta')^*}{E-\epsilon_{\mathbf{k}\lambda}+i\eta}, \tag{12}$$

where R and ζ index sites and $\eta=0^+$ gives the retarded function. As noted above, we are only interested in few elements of the matrix: diagonal and off-diagonal components involving sites 1, 4, 5, 8,…. Furthermore, there is extensive symmetry. We specifically examine $g_{s4l,4l'}=g_{s4l+1,4l'+1}$ and $g_{s4l,4l'+1}$.

In the TB model, the wave functions for the semi-infinite armchair CNT can be derived explicitly from those for the graphene sheet, as described in the Appendix. Using the expressions in Eqs. (A4)–(A7) for the amplitudes on the required sites, one can show that the components corresponding to $(\zeta=1,\zeta'=1)$ and $(\zeta=2,\zeta'=2)$ are given by

$$g_{s4l,4l'}(E)=g_{s4l+1,4l'+1}(E)=\frac{1}{\Omega}\sum_{\mathbf{k}}\sin^2\left(\frac{k_1}{2}\right)e^{i(2k_2-k_1)(l-l')}\times\left[\frac{1}{E-t|\gamma|+i\eta}+\frac{1}{E+t|\gamma|+i\eta}\right]. \tag{13}$$

The off-diagonal components $(\zeta=1,\zeta'=2)$ are given by

$$g_{s4l,4l'+1}(E)=\frac{1}{\Omega}\sum_{k}\frac{\gamma^*}{\gamma}\sin^2\left(\frac{k_1}{2}\right)e^{i(k_1-k_2)}e^{i(2k_2-k_1)(l-l')}\times\left[\frac{1}{E-t|\gamma|+i\eta}-\frac{1}{E+t|\gamma|+i\eta}\right]. \tag{14}$$

Both the ϵ_+ and ϵ_- branches are included. Under the $+k_y\rightarrow -k_y$ symmetry, the coefficient outside the square bracket goes to the complex conjugate so the summation on $\mathbf{k}$ can be restricted, taking the real part of the coefficient. With care for the bands at the Fermi energy, the general expressions have been evaluated numerically. They give results identical to those based on the recursion algorithm.

For a single point of attachment (e.g., for the polyene case in Fig. 2), we only need a single component, e.g., $g_{s1,1}$. Figures 3(a) and 3(b) show the real part and imaginary part of this component versus energy for the (5,5), (10,10), and (15,15) CNTs. The real part is linear near $E=0$ (the Fermi energy of the CNT), where it passes through zero, while the imaginary part is finite at $E=0$ with a weak quadratic part. At energies further removed from the Fermi energy, there is structure indicative of the Van Hove singularities in the CNT density of states.[21] As the CNT diameter increases, these peaks get closer to E_F. The slope in the real part near $E=0$ gets steeper. The magnitude of the imaginary part gets smaller, corresponding to the reduced density of states, as shown in Fig. 3(c). For two points of attachment, an off-diagonal component is also required. For example, the polyacene case depends on $g_{s1,4}$. For a junction bridged by two molecules, these off-diagonal components depend on the particular attachment points. In general, the off-diagonal coupling is only different for the cases where $(\zeta=1,\zeta'=2)$. As shown below, and illustrated in Fig. 3(d), these off-diagonal Green's function components depend on the angular separation of the attachment points. At $E=0$, they are purely real.

For the special case of $E=0$, further analytical results can be derived. From Eq. (13), the principal parts inside the square brackets cancel, leaving the residual δ function, and these surface Green's function components are purely imaginary:

$$g_{s4l,4l'}(E=0)=g_{s4l+1,4l'+1}(E=0)=\frac{-2i\pi}{\Omega}\sum_{\mathbf{k}}\sin^2\left(\frac{k_1}{2}\right)\times\cos[(2k_2-k_1)(l-l')]\delta(t|\gamma|). \tag{15}$$

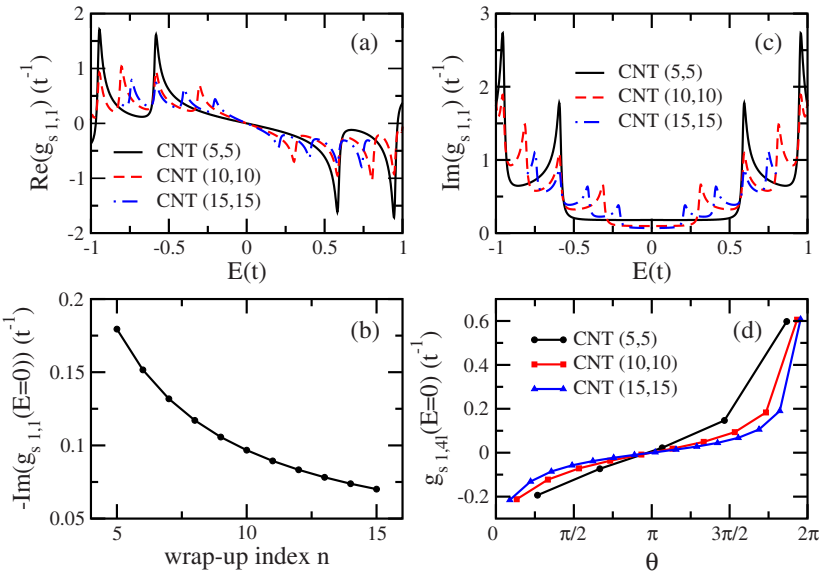

FIG. 3. (Color online) Properties of the armchair CNT surface Green's function. (a) Real and (b) imaginary parts of a diagonal component versus energy near the Fermi energy ($E=0$) for three different CNT diameters. (c) Variation of the imaginary part of the diagonal component at the Fermi energy with CNT diameter. (d) Off-diagonal component at the Fermi energy versus the separation of site $4l$ relative to site 1 expressed as an angle around the CNT circumference for three different CNT diameters, as illustrated in Fig. 2(b). The relation between the surface Green's function and the self-energy function is shown in Eq. (4).

For a graphene edge, the value is zero, following the vanishing density of states at $E=0$. For a CNT with a finite diameter, there is a finite density of states (DOS) and the integration yields

$$g_{s4l,4l'}(E=0) = g_{s4l+1,4l'+1}(E=0) = -i\frac{\sqrt{3}}{2nt} \equiv -i\delta. \quad (16)$$

As illustrated in Fig. 3(c), δ is inversely proportional to n. This result applies to all values of l; only the two bands passing through the CNT Fermi energy contribute to the value of δ. With reference to Fig. 2(b), the corresponding angular separation θ is zero for the diagonal case and $\theta = 2\pi/n, 4\pi/n, 6\pi/n, \ldots$ for the non-diagonal case.

For the other off-diagonal case [Eq. (14)], only the principal parts in the square brackets remain, showing that these components of the Green's function are purely real at $E=0$:

$$g_{s4l,4l'+1}(E=0) = \frac{-2}{t\Omega}\sum_k \frac{\gamma^*}{\gamma}\sin^2\left(\frac{k_1}{2}\right) \times e^{i(k_1-k_2)}e^{i(2k_2-k_1)(l-l')}P\left(\frac{1}{|\gamma|}\right) \equiv \nu(l-l'). \quad (17)$$

Since the dispersion goes through zero, care must be taken about the principal part. However, the integration in this region can be performed. For example, for the CNT case, the $m=0$ band contributes $-1/2n$ independent of l and l'. However, all of the bands also contribute, giving a smooth dependence on $l-l'$, as illustrated in Fig. 3(d). With reference to Fig. 2(b), the corresponding angular separations are $\theta = 4\pi/3n, 10\pi/3n, 15\pi/3n, \ldots$.

III. RESULTS FOR JUNCTION TRANSMISSION

A. Single polyene junctions

We first consider an idealized junction formed by simply removing all of the C sites from the central region of an armchair CNT, leaving a single strand of M sites with equal bond lengths and electronic hopping energy equal to that in the CNT electrodes ($t_s = t_d = t$). The orbital energies for the finite length, ideal polyene of length M can be derived from the corresponding band structure for the infinite polymer, as illustrated in Figs. 4(a) and 4(b). Imposing the boundary conditions of zero wave function at sites outside the finite chain yields the allowed states shown for M odd and even. The pattern of molecular levels is different. For M odd, there is always a molecular state at $E=0$ and with all other states occurring in pairs bracketing $E=0$. For M even, there is no

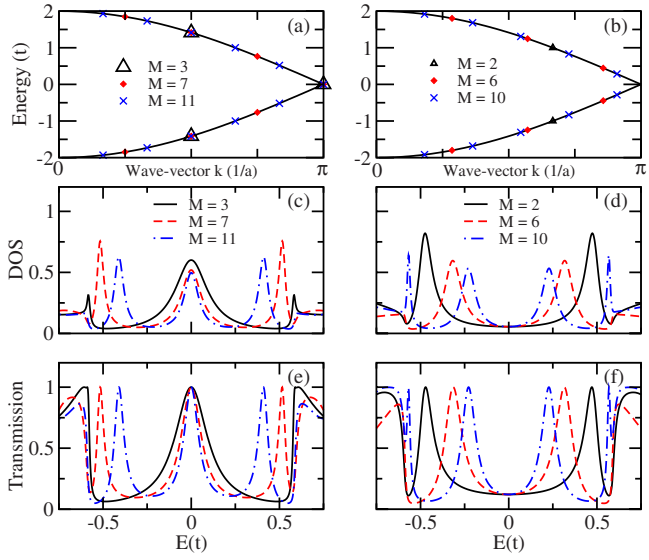

FIG. 4. (Color online) [(a) and (b)] Isolated polyene molecular orbital energies, [(c) and (d)] density of states (DOS), and [(e) and (f)] transmission for (5,5) CNT-polyene junctions with different molecular lengths. M is the number of carbons in the polyene molecule. In (a) and (b), the energy levels of isolated polyenes are shown as discrete points plotted on the continuous energy bands of the hypothetical infinite polyene chain. The wave vector k is expressed in terms of the unit cell length a.

state at $E=0$ and the nearest states bracket $E=0$ symmetrically with a gap that gets smaller with increasing chain length.

In the coupled system, this pattern is preserved in the energy region near $E=0$. The calculated local density of states in the molecule region and transmission are illustrated in Figs. 4(c)–4(f). The coupling to the electrodes both introduces a finite broadening and shifts the position of the resonance, through the self-energies in Eq. (4). In this case, only a single, diagonal component of the surface Green's function enters and the energy dependence is illustrated in Figs. 3(a) and 3(b). In the M odd case, a central peak occurs in the density of states and in the transmission. The real part of the self-energies is zero at $E=0$, so there is no shift, just a broadening. For longer chains, other, symmetrically disposed peaks are observed. For the M even case, only the symmetrically placed peaks are present. In both cases, the positions of the transmission peaks are shifted relative to the isolated polyene orbital energies. For example, for $M=2$, the isolated orbital energies are $\pm t$, but the final coupled resonance positions are closer to $\pm 0.5t$, shifted by the real part of the self-energy in Fig. 3(a). For energies more than about $0.5t$ from the Fermi energy of the CNT, structures from the Van Hove singularities in the CNT electrodes enter. The transmission at the Fermi energy ($E=0$) is always unity in the odd case, although the width of the transmission peak gets systematically narrower for longer chains. For the even cases, the transmission is constant, independent of chain length. However, it is specifically not unity.

In terms of the single component of the surface Green's function, $g_{s1,1}(E=0)=-i\delta$, the self-energies at the Fermi energy are just $\Sigma=-i\tau^2\delta$ [see Eq. (4)]. Using the recursion method, the transmission for a symmetric junction is just $T(E=0)=1$ for M odd and

$$T(E=0)=\frac{4\tau^4\delta^2 t^2}{(\tau^4\delta^2+t^2)^2} \tag{18}$$

for M even. For the ideal case considered in Fig. 4, the transmission for M even evaluates to $T(E=0)=48n^2/(3+4n^2)^2$ for (n,n) electrodes. The analytic solution verifies the length independence and the monotonically decreasing transmission in the even case as a function of CNT diameter. The length independence of the transmission can be understood with reference to the polymeric limit of the ideal polyene which does not have a band gap at $E=0$. As a consequence, the states near $E=0$ in the junction with a finite polyene segment do not exhibit exponential decay in the molecule region.[34]

More generally, the transmission maxima correspond to the DOS peaks in the energy range near $E=0$, before the onset of the Van Hove related structure, and correspond to one ideal channel, $T=1$. The uncut armchair CNT has two bands crossing at the Fermi energy. In the energy range between the nearest Van Hove singularities, there are just two electronic channels available for conductance. When a molecular resonance in the junction falls in this range, it opens exactly one channel for conductance. Although the peak transmission on the resonances is exactly unity, the width of the transmission resonances depends on the length of the chain. The recursion analysis can be extended to finite energy, small compared to t, for the odd M polyene to derive

$$T(E)=\frac{16\tau^4\delta^2/(M+1+2\tau^2\alpha)^2}{E^2+16\tau^4\delta^2/(M+1+2\tau^2\alpha)^2}, \tag{19}$$

where $\mathrm{Re}\, g_{s1,1}(E)=-\alpha E$ is assumed, following the results shown in Fig. 3(a) which suggest $\alpha\sim 1/t^2$. This illustrates the chain length dependence of the transmission resonances.

When the calculations are repeated with a finite value of η to represent the effects of dephasing on electrons transmitted through the junction, the transmission resonances are no longer unity at the peak. The recursion analysis shows that for the M odd case,

$$T(E=0,\eta\neq 0)=\frac{16\tau^4\delta^2}{[(M+1)\eta+4\tau^2\delta]^2}. \tag{20}$$

The dephasing leads not only to increased broadening of the resonance but also to reduced transmission at the peak.

So far, the analysis has focused on an idealized model where the single molecular strand was a fragment of the rigid CNT structure. In practice, a finite molecular wire with delocalized π states has lower energy with alternately bond lengths. For simplicity, the bonds are modeled as alternatively shorter and longer than the ordinary C–C bonds in the CNT, by equal amounts, resulting in $t_d=t+\Delta t$ and $t_s=t-\Delta t$. Furthermore, the electronic hopping energy between the end of the CNT and the π system of the molecule will be modified by the details of the chemical link (e.g., the amide linkage utilized in recent experiments[19]). This is modeled by varying τ. Finally, the C–C bond lengths will relax at the end of the armchair CNT as well. A limited exploration of the impact of CNT end relaxation suggests that it does not qualitatively influence the transmission characteristics.

The inclusion of the bond alternation leads to a numerically calculated transmission versus energy qualitatively similar to Fig. 4(d). However, the transmission at the Fermi energy depends on molecular length. It decreases exponentially as the polyene length increases. The bond alternation opens a gap of $4\Delta t$ in the band structure in the polymeric limit. As the parameters t_d and t_s are modified to open larger gaps in the DOS, the exponential decay constant increases. Analytically, the recursion method can be applied, with slightly more complicated iterates, to derive

$$T(E=0)=\frac{4\tau^4\delta^2 t_s^2 e^{\beta M}}{(\tau^4\delta^2+t_s^2 e^{\beta M})^2}, \tag{21}$$

where $\beta=2\ln(t_d/t_s)$. In the limit of large M, the transmission decays exponentially, $e^{-\beta M}$, as generally expected.[32,33] The expression for the decay constant agrees with previous studies.[34–36]

The impact of the link hopping between the CNT π system and the molecule (τ) depends on the magnitude of the surface Green's function, and hence the diameter of the CNT. For fixed link hopping, increased CNT diameter leads to reduced transmission at the Fermi energy for the bond alternated polyene. The broadening of the molecular resonances that bracket the Fermi energy is reduced [Eq. (16)]. Of

course, with reference to Eq. (21), this changes qualitatively for sufficiently large hopping parameter at the link to the CNT (τ). For the $\tau \ll t$ to $\tau \approx t$ regime, the transmission decreases as $1/d^2$, while for large hopping parameter, the transmission increases like d^2. In fact, for a given magnitude of the surface Green's function, the transmission can, in principle, be optimized to unity by proper choice of τ. In practice, the link bonding is very unlikely to lead to a hopping energy that exceeds the π electron hopping energy t within the CNT electrode.

B. Two-polyene junctions

In experiments, it is often unknown whether a single molecule or multiple molecules bridge the gap between the two electrodes. From the theoretical perspective, it is interesting to understand how quantum mechanical interference effects influence the transmission properties when multiple molecules occur in the junction.[37] The case of CNT electrodes considered here offers the advantage of well-defined, single points of attachment for the molecules. Furthermore, for the armchair CNT electrodes considered here, symmetry significantly simplifies the problem, enabling a clear picture. In this section, we analyze junctions bridged by two identical polyenes.

With reference to Fig. 2(a), the available attachment points are atoms 1,4,5,8,…. on the circumference. In general, the transmission depends on the two attachment points on the left and on the right: $T_{i,j;i',j'}(E)$. The left and right embedding self-energies will be 2×2 matrices and depend on the attachment points,

$$\Sigma_{i,j} = \begin{pmatrix} \tau & 0 \\ 0 & \tau \end{pmatrix} \begin{pmatrix} g_{si,i} & g_{si,j} \\ g_{sj,i} & g_{sj,j} \end{pmatrix} \begin{pmatrix} \tau & 0 \\ 0 & \tau \end{pmatrix}, \tag{22}$$

where the link coupling for the two polyenes is assumed to be the same for simplicity. As discussed in Sec. II C, there are two distinct symmetry types $(4l, 4l+1)$ according to the graphene sublattice from which they derive $(\zeta=1, \zeta=2)$. While the diagonal surface Green's function matrix elements are identical by symmetry, the off-diagonal elements connecting a pair of sites on the circumference depend on the symmetry type and the separation. This results in two distinct types of embedding self-energy to consider: when the attachment points are from the same sublattice,

$$\Sigma_{4l,4l'}(E=0) = \Sigma_{4l+1,4l'+1}(E=0) = \tau^2 \begin{pmatrix} -i\delta & -i\delta \\ -i\delta & -i\delta \end{pmatrix}, \tag{23}$$

and when the attachment points are from distinct sublattices,

$$\Sigma_{4l,4l'+1}(E=0) = \Sigma_{4l+1,4l'}(E=0) = \tau^2 \begin{pmatrix} -i\delta & \nu(l-l') \\ \nu(l-l') & -i\delta \end{pmatrix}. \tag{24}$$

We carefully distinguish three distinct types of junction formed by two bridging polyenes according to the attachment points on the left and on the right: (i) same sublattice left and right, (ii) different sublattice left and right, and (iii) same sublattice left and different sublattice right. Specific examples of cases (i) and (ii) are illustrated in Figs. 5(a) and 5(b), where the two bridging polyenes are parallel. Before we discuss each in turn, first note that for either case (i) or case (ii), a new basis can be chosen such that the space of the two contact points at each side is properly expressed in an odd channel and an even channel.

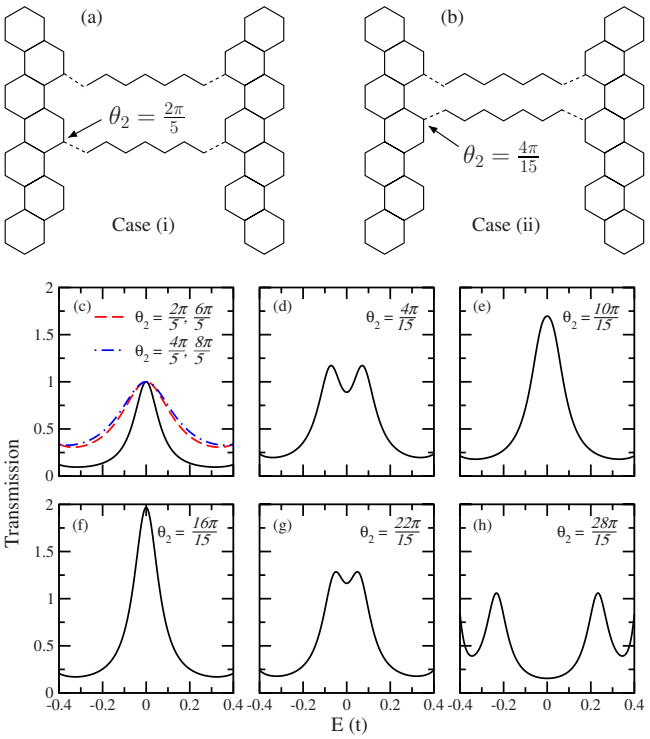

FIG. 5. (Color online) Transmission of two parallel $M=7$ ideal polyenes in the junction versus energy near the Fermi energy for (5,5) CNT electrodes. The same contact point combination is assumed for both the left and the right electrode, resulting in parallel molecules. One of the polyenes attaches to each lead at a point defined by $\theta_1=0$, while the other attaches to each lead at another point denoted as θ_2, with the angular measure defined in Fig. 3. The top panel visually illustrates the two distinct cases. (a) An example of case (i), where the two attachment points on each side are of the same sublattice, and (b) an example of case (ii), where the two attachment points are of different sublattices. (c) Transmission of case (i). For comparison, transmission is also shown for a single polyene in the junction. [(d)–(h)] Transmission of case (ii) for the specified values of θ_2.

For case (i), the embedding self-energy on the left and on the right [Eq. (23)] are independent of the specific indices of the attachment points (l, l') on the right or on the left. Furthermore, the self-energy matrix is singular. In the new basis,

$$\Sigma_{L(R)}(0) = \tau^2 \begin{pmatrix} -2i\delta & 0 \\ 0 & 0 \end{pmatrix}. \tag{25}$$

The odd channel has no coupling to the electrode and hence makes no contribution to the transmission. On the other hand, the self-energy for the even channel is exactly twice as large as the self-energy for a single polyene, $\Sigma(E=0) = -2i\tau^2\delta$. As a result, the transmission through two ideal M

odd polyenes in this case is still exactly unity at $E=0$, but exhibits twice the width. This is illustrated in Fig. 5(a). Furthermore, this argument generalizes to n ideal M odd polyenes in the junction, provided the attachment points to each electrode are from the same sublattice. For the case of two M even polyenes, Eqs. (18) and (21) apply for the ideal and bond alternated chains, respectively, upon substituting 2δ for δ. In the physically relevant regime of link coupling τ, the transmission for two molecules is enhanced relative to the single-molecule case. Thus, the quantum interference effects are quite simple in this case.

For case (ii), the embedding self-energy on the left and on the right [Eq. (24)] explicitly depend on the specific indices of the attachment points (l,l') on the right or on the left. In the new basis,

$$\Sigma_{L(R)}(0) = \tau^2 \begin{pmatrix} -i\delta + \nu_{L(R)} & 0 \\ 0 & -i\delta - \nu_{L(R)} \end{pmatrix}. \tag{26}$$

The recursive solution for the effective Green's function proceeds as before for the even and odd channels separately. The transmission is the sum of the contributions from the two channels. For the case of two ideal M odd polyenes,

$$T_{4l_L,4l'_L+1;4l_R,4l'_R+1}(E=0) = \frac{8\delta^2}{4\delta^2 + (\nu_L+\nu_R)^2}. \tag{27}$$

The real coupling $\nu(l-l')$ depends on the separation between the attachment points, as illustrated in Fig. 3(d). It governs the impact on the interference effects, as illustrated for the special case of $\nu_L=\nu_R$ shown in Fig. 6(a). The intersite coupling ν vanishes for π angular separation, resulting in two full channels of transmission, $T(E=0)=2$. However, where the coupling is nonzero, interference suppresses the transmission, even to a value less than that for a single molecule in the junction. Physically, the real intersite coupling through the CNT electrodes results in a shift of the resonances away from the Fermi energy. This is illustrated in Figs. 5(b)–5(f) for a few representative angles where the $T(E)$ can show a double peak structure.

For a pair of M even polyenes attached to the electrodes at points from different sublattices, the recursive solution yields

$$T_{4l_L,4l'_L+1;4l_R,4l'_R+1}(E=0) = \frac{8\tau^4\delta^2 t_s^2 e^{\beta M}}{(\tau^4\delta^2 - \tau^4\nu_R\nu_L + t_s^2 e^{\beta M})^2 + \tau^8\delta^2\nu_R\nu_L}. \tag{28}$$

This should be compared to the single polyene case in Eq. (21). In the limit of zero intersite coupling ν, the transmission is just doubled compared to a single molecule in the junction. As illustrated in Fig. 6(b), for a junction with $\nu_L=\nu_R$ and no bond alternation, the influence of the coupling through the electrodes is quite modest for the even polyene case. Physically, the even polyene already exhibits a gap in the spectrum at the Fermi energy. The additional splitting between the odd and even channels has a small effect.

For case (iii), the junction is asymmetrical with the left side attachment sites being from the same sublattice and the right side attachment sites being from opposite sublattices. In this case, although both even and odd channels are coupled to the right electrode, only the even channel couples to the left electrode. Thus, only the even channel contributes. For the M odd ideal polyene,

$$T_{4l_L,4l'_L;4l_R,4l'_R+1}(E=0) = \frac{8\delta^2}{9\delta^2 + \nu_R^2}. \tag{29}$$

Even in the limit of zero coupling through the CNT on the right, the transmission never exceeds unity due to the asymmetry of the junction. For the M even polyene,

$$T_{4l_L,4l'_L;4l_R,4l'_R+1}(E=0) = \frac{8\tau^4\delta^2 t_s^2 e^{\beta M}}{(2\tau^4\delta^2 + t_s^2 e^{\beta M})^2 + 4\tau^8\delta^2\nu_R^2}. \tag{30}$$

As in the M odd case, the asymmetry of the junction reduces the transmission relative to the symmetric case [Eq. (28)].

Since interference effects play a role in the transmission, it is interesting to ask the extent to which dephasing or structural fluctuations[28] alter those effects. The most sensitive example is case (ii) illustrated in Figs. 5 and 6. Physically, the fluctuations must shift the frontier molecular orbital energies by an amount comparable to the width or splitting illustrated in Fig. 5 to have a significant effect. This scale is set by the structure of the self-energies, e.g., Eq. (24). One would expect fluctuations in the orbital energies to be a relatively small fraction of the π hopping parameter t, of order $0.1t$. For the case of ideal coupling and CNT size illustrated in Fig. 6, small changes result (less than 10%). However, the effective coupling parameter τ could be relatively small, de-

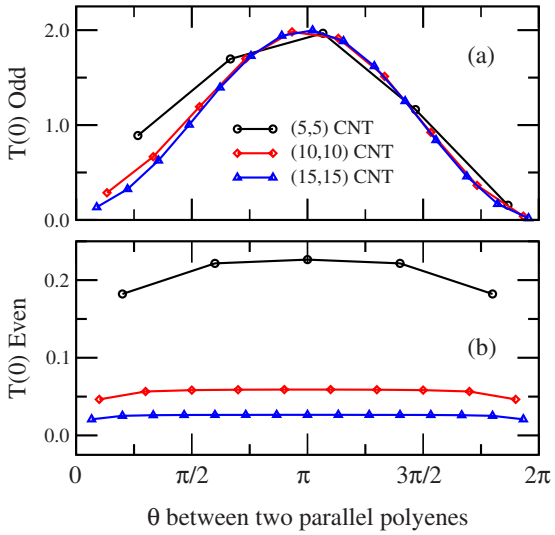

FIG. 6. (Color online) Transmission at the Fermi energy through a junction containing two ideal polyenes in case (ii) where the two attachment points on the left and on the right are from different sublattices. Symmetric junctions are assumed corresponding to parallel molecules in the junction. Transmission is plotted as a function of angular separation between the attachment points. Three different CNT electrodes are considered, as indicated. Ideal polyenes with (a) M odd and (b) M even are considered. The transmission is length independent.

pending on the details of the actual chemical link. In addition, δ is inversely proportional to the size of the CNTs, while the real couplings $\nu_L(R)$ only depend on the relative positions of the attachment points. For any given fluctuation, the ratio between the fluctuation and $\delta\tau^2$, as well as the ratio $(\nu_L+\nu_R)/\delta$, would compete to determine the interference. To fully analyze the expected transport through such narrow resonances, more details of the effect of fluctuations and dephasing processes would be necessary.

C. Polyacene junctions

The third type of junction illustrated in Fig. 1 consists of a series of fused rings (a polyacene) coupled to the CNT electrodes through two points of attachment at each end. To be more general, we consider the contact coupling (τ) separately and also allow for a distinct hopping along the edge of the polyacene (t_1) and between the edges (the upright rungs, t_2). We consider a series of junctions where the isolated polyacene corresponds to the molecules with $r=1,2,3,\ldots$ fused rings: benzene, naphthalene, anthracene, etc. In the simple TB model, the π electron orbital energies form a symmetric set with respect to $E=0$, illustrated in Fig. 7(a). The states are superposed on the band structure for the corresponding infinite polymer. Note that the states with zero energy at the zone boundary only exist in the polymeric limit, not being compatible with the boundary conditions for the π states of a finite molecule considered here. When coupled to the electrodes, the resulting resonances are shifted and broadened, just as for the polyene case. Numerical results for the transmission as a function of energy are illustrated in Fig. 7(b) for the ideal case of $\tau=t_2=t$.

The left and right electrode self-energies are of the same form as in Eq. (24), specifically $\Sigma_{1,4}$. The recursion calculation is simplified by considering the even and odd channels separately, for the contributions from the two species are just the same and independent. For a polyacene with r rings, the result for the transmission at the Fermi energy is

$$T(E=0)=\frac{8\tau^4\delta^2}{4\tau^4\delta^2+[2\tau^2\nu-(r+1)t_2]^2}, \tag{31}$$

which reduces to the result of a two M odd polyenes [Eq. (27)] when $t_2\to 0$, as it should. The real part of the self-energy is negative in this case (from Fig. 3, $\nu<0$). Therefore, as a function of molecular length (number of rings r), the transmission is less than unity and monotonically decreasing. As the number of rings is increased, the energy separation between the acene orbital energies gets smaller. This is illustrated in Fig. 7(b). However, the tunneling distance is also increasing so the transmission at $E=0$ does drop with the increasing acene length. However, the decrease is not exponential, as seen in Fig. 7(c). In this model, the band structure in the limit of an infinite polyacene chain does not have an energy gap. However, the bands forming the even and odd channels separately do have gaps. Their band edges coincide at $E=0$. Thus, the transmission is calculated just at the band edge. The result is the algebraic length dependence found here.

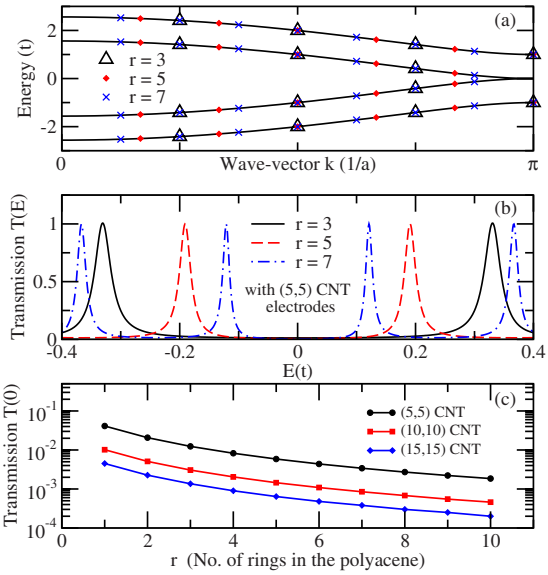

FIG. 7. (Color online) Polyacene transmission for the ideal case of all hopping equal to the CNT value t. (a) Molecular orbital energy levels of isolated polyacene molecules, plotted on the bands of the hypothetical infinite polyacene chain. The wave vector k is expressed in terms the unit cell length a. Note that the open triangles overlap other symbols. (b) Transmission versus energy near the Fermi energy for (5,5) CNT electrodes reconnected by $r=3$, 5, and 7 fused rings. (c) Transmission at the Fermi energy as a function of ring number for CNT electrodes of different diameters.

From experiment, it is not known whether the polyacenes show a gap in the limit of long chain length. DFT based calculations actually show a slight band overlap at the zone edge, indicative of a semimetal. Correcting for known errors in the DFT eigenvalues by evaluating the electronic correlation energy in the GW approximation suggests a finite gap.[38] In the present TB model, we illustrate this issue by introducing a third neighbor coupling t_3 across each ring parallel to the vertical rungs of the acene (Fig. 8). When $\text{sign}(t_3)=-\text{sign}(t_2)$, there is an energy gap between the even and odd bands nearest the Fermi energy ($E=0$). The numerical results for the transmission at the $E=0$ now show an exponential length dependence. If the sign is the same, these bands overlap with the Fermi energy ($E=0$) crossing both. For special values of length for the finite molecules, the resonances can fall near $E=0$, resulting in transmission resonances.

IV. CONCLUSION

Within a tight-binding model for the π electrons, the transmission $T(E)$ of simple prototype aromatic organic molecules covalently bonded to metallic CNT leads presents a tractable model problem in the field of single-molecule conductance studies. The examples we chose give a clear picture for the properties of the transmission, on resonance or off resonance, and the role of interference effects, for multiple molecules in the junction or for multiple contact points. These properties result from the interplay among CNT diameter, molecular length, contact strength and location, and the

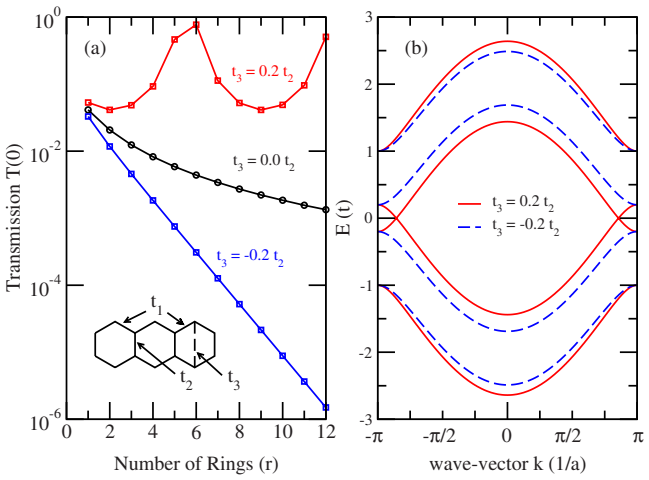

FIG. 8. (Color online) (a) Transmission $T(0)$ of polyacene junction as a function of molecular length, shown for different t_3 values. (b) The band structure of an infinite acene chain. By tuning t_3, the system changes from a semiconductor $[\text{sign}(t_3)=-\text{sign}(t_2)]$ to a semimetal $[\text{sign}(t_3)=\text{sign}(t_2)]$.

molecular dimerization. The basic results for transmission at the Fermi energy can be obtained analytically. This is supplemented by numerical calculations for the energy dependence of the transmission.

In the most ideal case, one can imagine the junction being formed by removing C atoms from the junction region, leaving one or more ideal strands. Even so, a single strand (ideal polyene) leads to unit transmission at the Fermi energy only in the case of an odd number of atoms. For two such strands, the transmission is sensitive to the details of the contact sites due to interference effects. The transmission approaches that of an infinite CNT $[T(E=0)=2]$ in special cases, while for other choices it can even yield $T(E=0)\rightarrow 0$. The odd and even symmetry channels result in resonances that are split in energy around the Fermi energy due to the coupling through the CNT electrodes. If instead, an ideal, bonded double strand (polyacene) forms the junction, the transmission at the Fermi energy is low, the opposite of a naive idea of restoring two full conductance channels. The resonances are separated from the Fermi energy for the ideal polyacene.

Results for these idealized junctions illustrate that achieving molecular junctions with a full quantum of conductance is more subtle than simply maintaining a well matched bonding network. The details of the quantum mechanical coupling can lead to quite varied transmission values because the specific bonding networks in the junction tend to result in resonances separated from the CNT electrode Fermi energy. Inclusion of more realistic details in the model, such as the bond alternation that is common in aromatic fragments, generally leads to transmission with off-resonance tunneling characteristics, e.g., exponential length dependence. More realistic treatment of the electrostatic potential profile (not considered here) will alter the quantitative characteristics, but not the overall picture. Finally, the case of semiconducting CNT electrodes, together with a back gate to tune the chemical potential, breaks the electron-hole symmetry and may offer more flexibility to achieve resonant tunneling conditions for molecular junctions.

While the CNT electrodes offer the opportunity for chemically well controlled junction formation, they also have a relatively low density of states at the Fermi energy. This results in modest broadening of the molecular resonances in the junction. With relatively sharp resonances, the conditions for resonant transmission, the condition under which a full quantum of conductance will be realized, become rather delicate to achieve. On the other hand, if an external control mechanism can be realized, this presents the opportunity for more sharply defined switching and other nonlinear conductance phenomena.

ACKNOWLEDGMENTS

We thank Louis Brus and Mike Steigerwald for helpful discussions and Chi-Lun Lee for technical advice. This work was primarily supported by the Nanoscale Science and Engineering Initiative of the National Science Foundation under NSF Award No. CHE-0117752 and the New York State Office of Science, Technology, Academic Research (NYSTAR). This work was partially supported by the MRSEC Program of the National Science Foundation under Grant No. DMR-0213574, the National Center for Theoretical Sciences (NCTS) of Taiwan, the National Science Council of Taiwan under NSC Project No. 95-2112-M-003-026-MY2, and the U.S. Department of Energy, Office of Basic Energy Sciences, under Contracts Nos. DE-FG02-90ER14152 and DE-AC02-98CH10886.

APPENDIX: ELECTRONIC STATES FOR SEMI-INFINITE (N,N) CARBON NANOTUBE

The (n,n) CNT surface Green's function in the text requires a formulation of the wave functions in the nearest neighbor TB model for the states which satisfy appropriate boundary conditions at the end of the semi-infinite tube. The graphene lattice and basic notation are illustrated in Fig. 2. The TB Hamiltonian for graphene at wave vector $\mathbf{k}$,

$$H(\mathbf{k}) \equiv t\begin{pmatrix} 0 & \gamma^* \\ \gamma & 0 \end{pmatrix} = t\begin{pmatrix} 0 & 1+e^{-i\mathbf{k}\cdot\mathbf{a}_1}+e^{-i\mathbf{k}\cdot\mathbf{a}_2} \\ 1+e^{i\mathbf{k}\cdot\mathbf{a}_1}+e^{i\mathbf{k}\cdot\mathbf{a}_2} & 0 \end{pmatrix},$$

$$|\gamma| = \sqrt{3+2[\cos\mathbf{k}\cdot\mathbf{a}_1+\cos\mathbf{k}\cdot\mathbf{a}_2+\cos\mathbf{k}\cdot(\mathbf{a}_1-\mathbf{a}_2)]},$$

yields eigenvalues and eigenvectors

$$\epsilon_{\mathbf{k},+} = t|\gamma|, \quad \xi_{\mathbf{k},+} = \frac{1}{\sqrt{2}|\gamma|}\begin{pmatrix} |\gamma| \\ \gamma \end{pmatrix},$$

$$\epsilon_{\mathbf{k},-} = -t|\gamma|, \quad \xi_{\mathbf{k},-} = \frac{1}{\sqrt{2}|\gamma|}\begin{pmatrix} \gamma^* \\ -|\gamma| \end{pmatrix},$$

corresponding to envelope wave functions (local orbital suppressed)

$$\psi_{\mathbf{k},\pm}(\mathbf{R},\zeta) = \frac{1}{\sqrt{\Omega}}e^{i\mathbf{k}\cdot\mathbf{R}}\xi_{\mathbf{k},\pm}(\zeta). \tag{A1}$$

The normalization factor here Ω is the total number of unit cells in the system.

An armchair edge is formed by cutting the graphene along the direction of vector $\mathbf{R}_\theta=\mathbf{a}_1-2\mathbf{a}_2$ (Fig. 2). The states for this semi-infinite system are developed from the degenerate states at $\pm k_x$ in the infinite graphene sheet:[39] $\mathbf{k}=k_1\frac{\mathbf{G}_1}{2\pi}+k_2\frac{\mathbf{G}_2}{2\pi}$ and $\mathbf{k}'=-k_1\frac{\mathbf{G}_1}{2\pi}+(k_2-k_1)\frac{\mathbf{G}_2}{2\pi}$:

$$\phi(\mathbf{k},\epsilon;\mathbf{R},\zeta)=c_1\psi_{\mathbf{k},\epsilon}+c_2\psi_{\mathbf{k}',\epsilon}. \tag{A2}$$

The boundary condition imposed requires the wave function in Eq. (A2) to be zero on the line of sites that fall just outside the edge in Fig. 2:

$$\phi(\mathbf{k},\epsilon;\mathbf{R}_0+l\mathbf{R}_\theta,\zeta=1)=0,$$

$$\phi(\mathbf{k},\epsilon;\mathbf{R}_1+l\mathbf{R}_\theta,\zeta=2)=0, \tag{A3}$$

where $\mathbf{R}_0=0$, $\mathbf{R}_1=-\mathbf{a}_2$, and l is any integer. With the coefficients $c_1=\frac{1}{\sqrt{\Omega/4}}\xi_{\mathbf{k}',\lambda}(1)$ and $c_2=-\frac{1}{\sqrt{\Omega/4}}\xi_{\mathbf{k},\lambda}(1)$, one can show that the boundary conditions are satisfied. Only those states indexed by $+k_x$ are unique.

The armchair CNT imposes periodic boundary conditions in the y direction (Fig. 2) such that the allowed $\mathbf{k}$ vectors satisfy $\mathbf{k}\cdot n\mathbf{R}_\theta=2m\pi$, restricting the hexagonal Brillouin zone summation to lines of $k_1-2k_2=2\pi\frac{m}{n}$.[13] The dispersion relation also exhibits $+k_y$ to $-k_y$ symmetry. The required surface Green's function components only involve sites $4l$ and $4l+1$. In terms of the graphene lattice, these correspond to $(\mathbf{R}=-\mathbf{a}_1+l\mathbf{R}_\theta,\zeta=2)$ and $(\mathbf{R}=-\mathbf{a}_2+l\mathbf{R}_\theta,\zeta=1)$, respectively. The necessary wave function components on these sites are given explicitly:

$$\phi(\mathbf{k},\epsilon_+;\mathbf{R}=-\mathbf{a}_2+l\mathbf{R}_\theta,\zeta=1)=\frac{1}{\sqrt{\Omega/4}}\frac{1}{2}\left(e^{i[lk_1-(2l+1)k_2]}-e^{-i[lk_1+(2l+1)(k_2-k_1)]}\right), \tag{A4}$$

$$\phi(\mathbf{k},\epsilon_+;\mathbf{R}=-\mathbf{a}_1+l\mathbf{R}_\theta,\zeta=2)=\frac{1}{\sqrt{\Omega/4}}\frac{1}{2|\gamma|}\left(\gamma e^{i[(l-1)k_1-2lk_2]}-\gamma' e^{-i[(l-1)k_1+2l(k_2-k_1)]}\right), \tag{A5}$$

$$\phi(\mathbf{k},\epsilon_-;\mathbf{R}=-\mathbf{a}_2+l\mathbf{R}_\theta,\zeta=1)=\frac{1}{\sqrt{\Omega/4}}\frac{1}{2|\gamma|^2}\left(\gamma'^*\gamma^* e^{i[lk_1-(2l+1)k_2]}-\gamma^*\gamma'^* e^{-i[lk_1+(2l+1)(k_2-k_1)]}\right), \tag{A6}$$

$$\phi(\mathbf{k},\epsilon_-;\mathbf{R}=-\mathbf{a}_1+l\mathbf{R}_\theta,\zeta=2)=\frac{1}{\sqrt{\Omega/4}}\frac{1}{2|\gamma|}\left(-\gamma'^* e^{i[(l-1)k_1-2lk_2]}+\gamma^* e^{-i[(l-1)k_1+2l(k_2-k_1)]}\right). \tag{A7}$$

Here, $\gamma=\gamma_{\mathbf{k}}$ and $\gamma'=\gamma_{\mathbf{k}'}=e^{-ik_1}\gamma$.

*yrchen@ntnu.edu.tw
†mhyberts@bnl.gov

[1] A. Nitzan and M. A. Ratner, Science **300**, 1384 (2003).
[2] A. Salomon, D. Cahen, S. Lindsay, J. Tomfohr, V. B. Engelkes, and C. D. Frisbie, Adv. Mater. (Weinheim, Ger.) **15**, 1881 (2003).
[3] A. Ulman, Chem. Rev. (Washington, D.C.) **96**, 1533 (1996).
[4] F. Schreiber, J. Phys.: Condens. Matter **16**, R881 (2004).
[5] H. Basch, R. Cohen, and M. A. Ratner, Nano Lett. **5**, 1668 (2005).
[6] G. S. Tulevski, M. B. Myers, M. S. Hybertsen, M. L. Steigerwald, and C. Nuckolls, Science **309**, 591 (2005).
[7] M. Siaj and P. H. McBreen, Science **309**, 588 (2005).
[8] L. Venkataraman, J. E. Klare, I. W. Tam, C. Nuckolls, M. S. Hybertsen, and M. Steigerwald, Nano Lett. **6**, 458 (2006).
[9] L. Venkataraman, J. E. Klare, C. Nuckolls, M. S. Hybertsen, and M. L. Steigerwald, Nature (London) **442**, 904 (2006).
[10] F. Chen, X. Li, J. Hihath, Z. Huang, and N. J. Tao, J. Am. Chem. Soc. **128**, 15874 (2006).
[11] S. Iijima and T. Ichihashi, Nature (London) **363**, 603 (1993).
[12] D. S. Bethune, C. H. Klang, M. S. De Vries, G. Gorman, R. Savoy, J. Vazquez, and R. Beyers, Nature (London) **363**, 605 (1993).
[13] N. Hamada, S. I. Sawada, and A. Oshiyama, Phys. Rev. Lett. **68**, 1579 (1992).
[14] H. J. Dai, Surf. Sci. **500**, 218 (2002).
[15] P. Avouris, J. Appenzeller, R. Martel, and S. J. Wind, Proc. IEEE **91**, 1772 (2003).
[16] P. F. Qi, A. Javey, M. Rolandi, Q. Wang, E. Yenilmez, and H. J. Dai, J. Am. Chem. Soc. **126**, 11774 (2004).
[17] K. Tsukagoshi, I. Yagi, and Y. Aoyagi, Appl. Phys. Lett. **85**, 1021 (2004).
[18] X. F. Guo, M. Myers, S. Xiao, M. Lefenfeld, R. Steiner, G. S. Tulevski, J. Tang, J. Baumert, F. Leibfarth, J. T. Yardley, M. L. Steigerwald, P. Kim, and C. Nuckolls, Proc. Natl. Acad. Sci. U.S.A. **103**, 11452 (2006).
[19] X. F. Guo, J. P. Small, J. E. Klare, Y. L. Wang, M. S. Purewal, I. W. Tam, B. H. Hong, R. Caldwell, L. M. Huang, S. O'Brien, J. M. Yan, R. Breslow, S. J. Wind, J. Hone, P. Kim, and C. Nuckolls, Science **311**, 356 (2006).
[20] S. Datta, *Quantum Transport: Atom to Transistor* (Cambridge University Press, New York, 2005).
[21] R. Saito, M. Fujita, G. Dresselhaus, and M. S. Dresselhaus, Phys. Rev. B **46**, 1804 (1992).
[22] K. Wakabayashi, Phys. Rev. B **64**, 125428 (2001).
[23] K. Wakabayashi and T. Aoki, Int. J. Mod. Phys. B **16**, 4897 (2002).
[24] K. Wakabayashi and M. Sigrist, Phys. Rev. Lett. **84**, 3390 (2000).
[25] G. Fagas, G. Cuniberti, and K. Richter, Phys. Rev. B **63**, 045416 (2001).
[26] R. Gutierrez, G. Fagas, G. Cuniberti, F. Grossmann, R. Schmidt, and K. Richter, Phys. Rev. B **65**, 113410 (2002).
[27] R. R. Pandey, N. Bruque, K. Alam, and R. K. Lake, Phys. Status Solidi A **203**, R5 (2006).

[28] M. Gheorghe, R. Gutierrez, N. Ranjan, A. Pecchia, A. Di Carlo, and G. Cuniberti, Europhys. Lett. **71**, 438 (2005).
[29] A. R. Williams, P. J. Feibelman, and N. D. Lang, Phys. Rev. B **26**, 5433 (1982).
[30] T. Ando, Phys. Rev. B **44**, 8017 (1991).
[31] F. Zahid, M. Paulsson, and S. Datta, in *Advanced Semiconductors and Organic Nano-Techniques*, edited by H. Morkoc (Academic, London, 2003), Pt. III, pp. 1–42.
[32] H. M. McConnell, J. Chem. Phys. **35**, 508 (1961).
[33] A. Nitzan, Annu. Rev. Phys. Chem. **52**, 681 (2001).
[34] A. Onipko and Y. Klymenko, J. Phys. Chem. A **102**, 4246 (1998).
[35] M. Magoga and C. Joachim, Phys. Rev. B **56**, 4722 (1997).
[36] M. Magoga and C. Joachim, Phys. Rev. B **57**, 1820 (1998).
[37] M. Magoga and C. Joachim, Phys. Rev. B **59**, 16011 (1999).
[38] T. A. Niehaus, M. Rohlfing, F. Della Sala, A. Di Carlo, and Th. Frauenheim, Phys. Rev. A **71**, 022508 (2005).
[39] M. Fujita, K. Wakabayashi, K. Nakada, and K. Kusakabe, J. Phys. Soc. Jpn. **65**, 1920 (1996).